# Trigonal Tellurium Nanostructure Formation Energy and Band gap

*Aaron Kramer[1], Maarten L. Van de Put[2], Christopher L. Hinkle[3], and William G. Vandenberghe[2]*

[1]Department of Physics and [2]Department of Materials Science and Engineering,
University of Texas at Dallas, 800 W. Campbell Rd., Richardson, Texas 75080, USA
[3]Department of Electrical Engineering, University of Notre Dame, Notre Dame, Indiana 46556, USA

***Abstract*—Trigonal-Tellurium (t-Te), a van der Waals material, recently garnered interest to the nanoelectronics community because a high hole mobility, a high bandgap, and low temperature growth have all been observed in nanostructures. We analyze various t-Te nanostructures (nanowires and layers) using first principles simulations. We compare bandgap variation and relative stability among different shapes and sizes of Te nanostructures. We determine that nanowires host higher bandgaps and are preferentially grown, rather than layers of t-Te. We also propose a simplified model using the number of van der Waals interactions in explaining relative stability among t-Te nanostructures. Finally, we study uniquely shaped (auxiliary) t-Te nanostructures and verify that their stability obeys the same simplified model.**

## I. Introduction

As semiconductor devices shrink in size, common materials such as silicon have their mobilities reduced significantly [1]. Graphene offers a solution to the low mobility problem, but unfortunately does not offer a bandgap [2]. An alternative material of interest to the nanoelectronics community is trigonal tellurium (t-Te), which admits a high hole mobility even in nanostructures [3]. While t-Te, in contrast to graphene, does offer a nearly direct bulk bandgap, the bandgap is small (0.33 eV) [4]. However, at scaled dimensions, quantum confinement results in an increasing bandgap and this may reduce leakage current and improve tellurium's prospects for use in future transistors.

Structurally, t-Te comprises of one-dimensional (1D) helical chains with covalently bonded Te atoms. These Te-helices manifests into a trigonal lattice though a mixture of van der Waals (vdW) interactions and covalent bonding. The overall trigonal structure, vdW interactions, and the covalent bonding are all consequences of Tellurium containing six valence electrons [5]. Historically t-Te was used in infrared detectors [6], thermoelectric [7], piezoelectric [8] and photoconductive devices [9].

Low-dimensional Tellurium allotropes, such as monolayer Tellurene have been investigated using first principles density functional theory (DFT). Notable allotropes are described in Zhu et. al. ($\alpha$, $\beta$, and $\gamma$) [10], Liu, Lin and Tomanek ($\delta$ and $\eta$) [11], and Xian et. al. (square Tellurene) [12]. It is worth mentioning that only the $\beta$ allotrope bears resemblance to bulk t-Te. For monolayers, the $\alpha$, $\delta$, and $\eta$ allotropes are predicted to be more stable than the $\beta$-allotropes with the $\eta$ allotrope being the most stable. Due to the approximations made in the DFT-treatment of the vdW interaction, determining the most stable t-Te nanostructure is challenging. Notably, different vdW models can change the order of the most stable monolayer structure.

Here we employ first principles calculations with DFT to compare and analyze the stability of various t-Te nanostructures (layers of t-Te and nanowires). We calculate formation energies, study surface-to-volume ratios, and develop a simplified model to determine the stability of 1D nanostructure using the total energy associated with a Te-helix with *m* helical-neighbors. We find that 1D hexagonal shaped nanowires are the most favored thermodynamically. We also include bandgaps and find that 1D triangle shaped nanowires feature the highest bandgaps (up to 1-2 eV) making t-Te an eye-catching channel material for extremely scaled field-effect transistors.

Section II contains our results and discussion, section III describes our methodology and section IV is our conclusion.

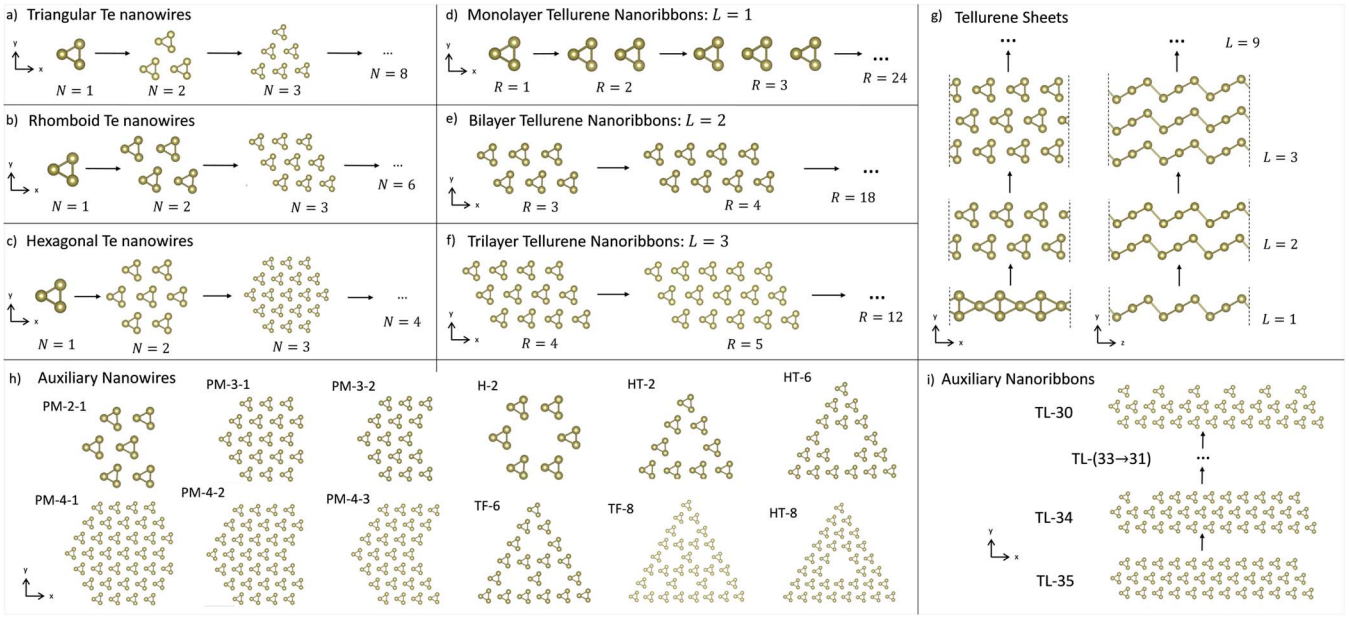


Figure 1. Illustration of all our computed t-Te nanostructures. Cross-sectional area of triangular (a), rhomboid (b), hexagonal (c) nanowires, and monolayer (d), bilayer (e), and trilayer (f) Tellurene nanoribbons, sheets of Tellurene (g), and auxiliary nanowires (h), and (i) nanoribbons. *N* is the number of helices per nanowire side. *R* is the number of helices on the longer nanoribbon side. *L* is number of layers for Tellurene sheets.

978-1-7281-0940-4/19/$31.00 ©2019 IEEE

## II. Results and Discussion

Fig. 1 illustrates all t-Te nanostructures under investigation. We have three classes of nanowires (triangular, rhomboid, and hexagonal), three classes of nanoribbons (monolayer, bilayer, and trilayer), and monolayer to multilayer sheets of Tellurene. Additionally, we create some "auxiliary" nanowires and nanoribbons to supplement our main structures.

### *A. Formation Energy*

Fig. 2 shows the calculated formation energies for all nanowires and nanoribbons. The nanoribbons have a higher formation energy than the nanowires for the same number of Te-helices. The order going from highest to lowest formation energy for the same number of Te helices is: monolayer (1L), bilayer (2L), and trilayer (3L) nanoribbons, then Triangular, Rhomboid, and Hexagonal nanowires.

Rhomboid nanowires would be the most difficult Te nanowire to fabricate because hexagonal or triangular nanowires would be preferentially formed instead, depending on the environment. This is in line with earlier experimental findings [13].

Finally, Fig. 2 shows that the monolayer (1L) ribbon has an exceedingly high formation energy and will be very difficult to fabricate unless substrate interactions drastically alter formation energies. The 2L and 3L ribbons have formation energies much closer to those of the wires and may form in the presence of favorable substrate interaction. Note that the monolayer, shown in Fig 1g, has a fundamentally different structure. 1L nanoribbons approach this limit as they get wider, while the helices in 2L and 3L ribbons remain structurally similar to bulk t-Te.

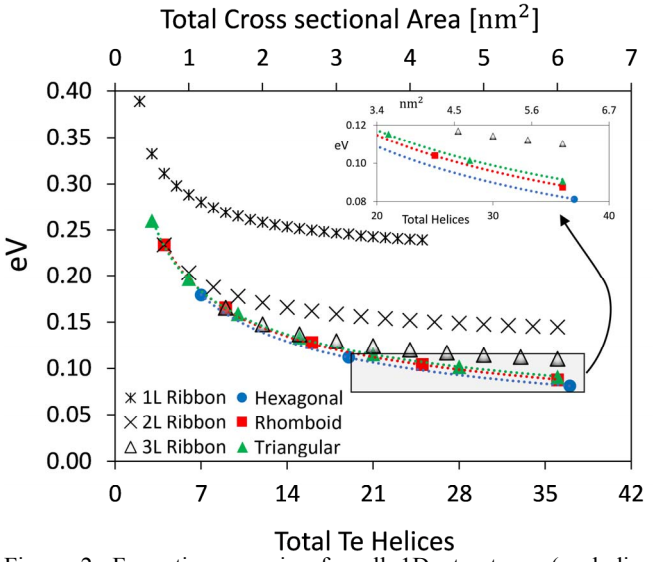


Figure 2. Formation energies for all 1D structures (excluding auxiliary structures) as a function of the total number of Te helices or cross-sectional area. The solid or open points are computed values. The dotted lines are power fits to guide the eye.

Table 1 shows the formation energy for the auxiliary structures and Tellurene sheets shown in Fig. 1h and 1g. Two auxiliary nanowires (e.g., PM-2-1 and H-2) can have the same number of helices (e.g., 6 helices) but vastly different formation energies (e.g., 0.20 eV/atom and 0.27 eV/atom). These structures do not follow the simple trend of nanowire formation energy in Fig. 2, where formation energy variation is small across the triangular, rhomboid, and hexagonal nanowires as the number of helices is varied.

The first three rows in Table 1b represent the lowest formation energies that monolayer, bilayer and trilayer nanoribbons can obtain. The formation energy quickly decreases with increasing number of layers. At around 7 layers the formation energy decrease starts to taper as the layers more closely resemble bulk.

(a) Auxiliary Structures

| Name | # of Helices | | Formation Energy [eV / atom] |
|---|---|---|---|
| PM-2-1 | 6 | | 0.20 |
| PM-3-1 | 18 | | 0.12 |
| PM-3-2 | 15 | Wires | 0.14 |
| H-2 | 6 | | 0.27 |
| HT-2 | 9 | | 0.21 |
| HT-6 | 18 | | 0.17 |
| PM-4-1 | 36 | | 0.08 |
| PM-4-2 | 34 | | 0.09 |
| PM-4-3 | 28 | | 0.10 |
| TF-6 | 18 | | 0.18 |
| TF-8 | 30 | | 0.16 |
| HT-8 | 33 | | 0.12 |
| TL-35 | 35 | | 0.11 |
| TL-34 | 34 | Ribbons | 0.12 |
| TL-33 | 33 | | 0.12 |
| TL-32 | 32 | | 0.13 |
| TL-31 | 31 | | 0.14 |
| TL-30 | 30 | | 0.14 |

(b) Tellurene Sheets

| Name | Formation Energy [eV / atom] |
|---|---|
| 1-Layer | 0.22 |
| 2-Layer | 0.13 |
| 3-Layer | 0.09 |
| 4-Layer | 0.07 |
| 5-Layer | 0.06 |
| 6-Layer | 0.05 |
| 7-Layer | 0.04 |
| 8-Layer | 0.04 |
| 9-Layer | 0.03 |

Table 1. a) The Formation energy of the auxiliary structures with the number of Helices present and b) 2D sheets of Tellurene.

To support our knowledge of the relative formation energies among nanostructures in Fig. 2, we calculate the surface-to-volume ratio, for all nanowires and the bilayer and trilayer nanoribbons (the auxiliary structures are excluded). The calculated surface-to-volume ratios are shown in Fig 3. Hexagonal nanowires have the smallest surface-to-volume ratio for the same number of helices. This agrees with Fig. 2 where hexagonal nanowires also have the lowest formation energy for the same number of helices. Unfortunately, surface-to-volume ratio does not illustrate all formation energy differences. For instance, the bilayer and trilayer nanoribbons have a lower surface-to-volume ratio compared to the triangular nanowires when the nanoribbons have more than 14 and 27 helices respectively. Since the nanowires in Fig. 2 always exhibit a lower formation energy compared to the nanoribbons, surface-to-volume ratio does not tell the full story.

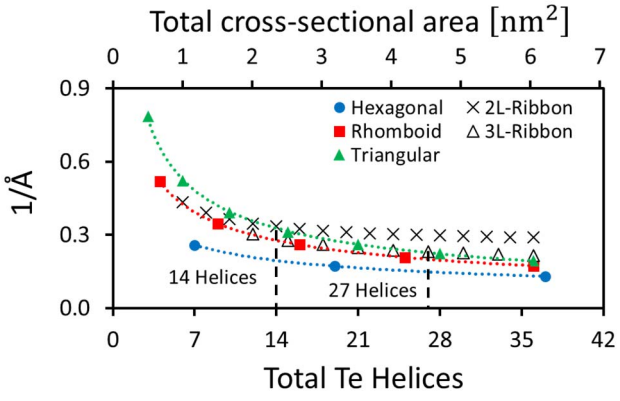


Figure 3. Surface-to-volume ratio for the nanowires and the nanoribbons. Solid points are calculated values and dotted lines are power fits to guide the eye.

An alternative explanation is in the differing number of "happy" helices that have six nearest helical-neighbors. Nanowires will always have more "happy" helices compared to nanoribbons for the same total number of helices. To determine whether the number of neighboring helices is a good metric, we determine an energy penalty $\epsilon_m$ associated with each helix that has a given number ($m$) helices.

Table 2 shows the resulting energy penalties determined using an ordinary least squares (OLS) fit as explained in the methods section. Significant energy penalties ranging from 1.17 eV to 0.39 eV are observed for helices with six to one missing helical-neighbors respectively. The small value $\epsilon_6 = 0.02$ eV indicates that the energy obtained from the OLS for helices with six helical-neighbors, is remarkably close to that of the bulk t-Te. To rule out large systematic errors between nanowire types, we verify that the order of largest to lowest formation energies observed in Fig. 2 is maintained using the energy penalties. We find that the formation energies of the auxiliary structures in Table 1a, the ones not used in the OLS fit, can be estimated within 3% error using the energy penalties.

Keeping the missing neighboring helix picture in mind, we inspect the results in Fig. 2 and Table 1. Our triangular, rhomboid, and hexagonal nanowires have Te-helices with fewer missing helical neighbors compared to layers of Tellurene. Our auxiliary structures have a large number of Te helices with many missing helical neighbors. Therefore, the missing neighboring helix picture, in contrast to surface-to-volume ratio picture, can explain why nanowires have lower formation energy than layers for the same number of Te-helices. As noted before, this agrees with experimental growth, which also found that wires rather than layers are preferred [3].

| | Energy Penalty [eV /Unit-Cell] |
|---|---|
| $\epsilon_0$ | 1.17 |
| $\epsilon_1$ | 0.89 |
| $\epsilon_2$ | 0.88 |
| $\epsilon_3$ | 0.55 |
| $\epsilon_4$ | 0.40 |
| $\epsilon_5$ | 0.39 |
| $\epsilon_6$ | 0.02 |

Table 2. The energy penalties for having $m$ helical-neighbors per unit cell determined using the OLS fit on all our structures. The energy penalty is relative to bulk t-Te.

### B. Electronic Properties

The computed bandgaps in Fig. 4 ranges from 0.34 eV to 1.46 eV. When interpreting these bandgaps, the tendency for DFT to underestimate the bandgaps should be taken in mind. For example, DFT predicts a vanishing t-Te bulk bandgap. The bandgap for the N=2 Hexagonal nanowire (Fig 1c N=2, 7 Helices) with hybrid HSE06 functionals [14] went from 0.50 eV to 0.99 eV, that is about a factor of 2.

Trends in nanowire bandgaps in Fig. 4 show that hexagonal, rhomboid, and triangular nanowires have lowest, intermediate, and the highest bandgaps respectively. Bandgap values start to decrease quickly at nanowire sizes around 7 helices ($\sim$1.3 nm$^2$).

The computed bandgaps for the auxiliary nanowires and sheets of Tellurene are given in Table 3. The auxiliary nanowires and sheets of Tellurene have their bandgap range from 0.37 eV to 0.94 eV and 0.17 eV to 1.01 eV respectively. Unlike the nanowires in Fig. 4 where bandgaps start to decrease quickly at a size of 7 Te helices ($\sim$1.3 nm$^2$), the auxiliary nanowires do not exactly follow that same decreasing trend at 7 Te helices. For instance, the TF-8 nanowire has 30 Te helices ($\sim$4.8 nm$^2$) but exhibits a high bandgap of 0.74 eV.

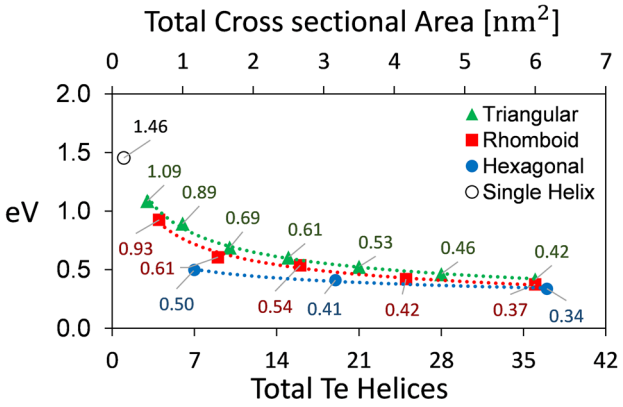


Figure 4. Bandgap values for our Triangular, rhomboid and hexagonal nanowires as a function of the total number of Te helices or total nanowire cross sectional area. Solid and open points are calculated points while the dotted lines are power and logarithmic fits to guide the eye.

(a) Auxiliary Nanowires

| Name | # of Helices | Bandgaps [eV] |
|---|---|---|
| PM-2-1 | 6 | 0.64 |
| PM-3-1 | 18 | 0.45 |
| PM-3-2 | 15 | 0.50 |
| H-2 | 6 | 0.57 |
| HT-2 | 9 | 0.94 |
| HT-6 | 18 | 0.79 |
| PM-4-1 | 36 | 0.37 |
| PM-4-2 | 33 | 0.45 |
| PM-4-3 | 28 | 0.41 |
| TF-6 | 18 | 0.85 |
| TF-8 | 30 | 0.74 |
| HT-8 | 33 | 0.58 |

(b) Tellurene Sheets

| Name | Bandgaps [eV] |
|---|---|
| 1-Layer | 1.01 |
| 2-Layer | 0.76 |
| 3-Layer | 0.58 |
| 4-Layer | 0.44 |
| 5-Layer | 0.35 |
| 6-Layer | 0.28 |
| 7-Layer | 0.24 |
| 8-Layer | 0.20 |
| 9-Layer | 0.17 |

Table 3. The computed bandgaps for a) auxiliary nanowires and b) sheets of Tellurene.

## III. Methodology

### A. Computational Details

We employ DFT as implemented in the Vienna Ab initio Simulation Package (VASP) [15], using the generalized gradient approximated PBE functional [16], DFT-D3 vdW corrections [17], and a 200 eV kinetic energy cutoff for the plane wave basis. For charge density calculations: all nanowires, nanoribbons, sheets of Tellurene, and the bulk t-Te use a 1x1x4, 1x1x4, 6x1x4, and 6x6x4 Monkhorst-Pack k-point sampling, respectively [18].

We relax the atomic positions of the bulk t-Te until all forces are lower than 0.005 eV/Å. From the bulk t-Te atomic coordinates and lattice parameters we construct and relax three classes of nanowires (Triangular, Rhomboid, and Hexagonal), three classes of nanoribbons (monolayer, bilayer, and trilayer), and monolayer to multilayer sheets of Tellurene. All auxiliary structures also created in the same

manner with the bulk t-Te atomic coordinates and lattice parameters.

The formation energy is $E_F = E_{\text{tot}}/N_{\text{tot}} - \epsilon_{\text{bulk}}$. Where $E_{\text{tot}}$ is the total ground state energy of a nanostructure, $N_{\text{tot}}$ is the total number of atom per supercell of a nanostructure, and $\epsilon_{\text{bulk}}$ is the cohesive energy of the bulk t-Te.

For bandgap calculations we sampled the first Brillouin zone with no less than 16 points between each symmetry point. Due to the relatively high mass of Tellurium we included spin-orbit coupling using methods developed by reference [19].

### B. Surface-to-Volume Ratio

For surface-to-volume-ratio calculations, we use lattice constants ($c$) plus a "quasi-lattice-constant" ($\tilde{a}$) in the non-periodic directions.

To calculate $\tilde{a}$ we separate all Te atoms into three planes normal to the z-axis. Within each plane, we calculate and then average out all the nearest neighbor distances $d_{p,i}$ for each atom in the plane. Where $i$ is the nearest neighbor atom (in terms of distance) index and $p$ is the plane index. The average nearest neighbor distances across all three planes is the quasi lattice constant. As a closed form equation, the quasi-lattice-constant is:

$$\tilde{a} = \frac{1}{3N_i}\sum_{p=1}^{3}\sum_{i=1}^{N_i} d_{p,i} \qquad (1)$$

$N_i$ equals the total number of nearest neighbor distance per plane. Figure 2 illustrates the methodology for the N=3 rhomboid t-Te nanowire.

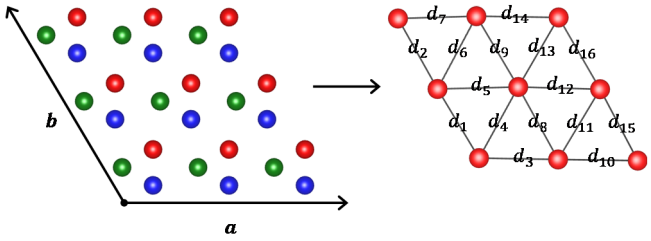


Figure 5. Calculation of $\tilde{a}$ for the N=3 Rhomboid nanowire. All green, blue, and red atoms are in separate planes. There are 16 distances in plane containing red atoms. There are 48 distances to average when calculating $\tilde{a}$ for the N=3 Rhomboid nanowire example when considering all three planes.

The surface-to-volume ratio for all nanowires and nanoribbons is $A_L/V$, where $A_L$ is the lateral surface area and $V$ is the volume occupied by the structure. The volume for the nanowires and nanoribbons is $V = A_B c$ where $A_B$ is the base area and $c$ is the lattice constant in the z-direction. The nanowire base area is either a hexagon ($A_B = 3\sqrt{3}(N\tilde{a})^2/2$), rhombus ($A_B = \sqrt{3}(N\tilde{a})^2/2$), or an equilateral triangle ($A_B = \sqrt{3}(N\tilde{a})^2/4$). The nanoribbon base areas are parallelograms ($A_B = LRa_{\text{bulk}}/2$), where $a_{\text{bulk}}$ is the bulk lattice constant which we calculate as 4.40 Å. Monolayer ribbons lack a consistent definition of a quasi-lattice constant, so we do not determine their surface-to-volume ratio.

To calculate the lateral surface areas, we use six ($N_R$=6), four ($N_R$=4), and three ($N_R$=3) rectangles for the hexagonal, rhomboid, and triangular nanowire supercells, respectively. The total lateral surface area is $A_L = N_R N\tilde{a}c$ where $N_R$ is the number of rectangles and $N$ is the number of Te-helices per nanowire side. The lateral surface for the nanoribbons is computed in the same manner using rectangles. Their total lateral surface area is approximated as $A_L \approx 2N_L a_{\text{bulk}}c + 2Ra_{\text{bulk}}c$.

### C. Formation Energy of a Te-Helix

We develop a simpler model of the formation energy by decomposing the formation energy $E_F$ of a 1D Te nanostructure as an energy penalty per Te-helix, based on its number of helical neighbors. If the energy penalty of a Te-helix with $m$-helical neighbors is given by $\epsilon_m$, the total formation energy is approximated by

$$E_{\text{tot}} \approx \sum_{m=1}^{6} \frac{n_m \epsilon_m}{N_{\text{tot}}} \qquad (2)$$

where $n_m$ is the number of Te helices with $m$ nearest helical neighbors in the structure.

We obtain the energy parameters $\epsilon_m$ by performing an ordinary least squares (OLS) fit on Eq. (2) for $m > 1$. We fit the parameters on the calculated formation energies for all 1D structures in Fig. 1, excluding the auxiliary nanoribbons. The energy penalty $\epsilon_0$ is simply the total energy difference between a single Te helix and a helix in the bulk t-Te.

## IV. Conclusion

Our calculations have shown that hexagonally shaped t-Te nanowires are the most thermodynamically stable, while triangular shaped nanowires can host high bandgaps while still being thermodynamically stable. Layers of t-Te are not favorable to be grown compared to the nanowires. Nanowires are more stable than layers of t-Te because nanowires allow more vdW interactions per Te-helix. Based on the number of neighbors of a Te-helix, we create a simple model to predict the formation energy of any nanostructure of t-Te. Computing the bandgap, we show that small nanowires can have a bandgap of more than 1 eV for a cross section lower than around 1 nm$^2$, making Te a promising material for future nanoelectronic applications.

## References


[1] F. Gamiz and M. V. Fischetti, *J. Appl. Phys*, **89**, 5478 (2001)
[2] A. H. C. Neto, et al., *Rev. Mod. Phys*., **81**, 109 (2009)
[3] G. Zhou, et al., *Adv. Mater.* **30**, 1803109 (2018)
[4] V. B. Anzin, et al., *Phys. Status solidi*, **42**, 385 (1977)
[5] J. D. Joannopoulos, et al., *Phys. Rev. B*, **11**, 2186 (1975)
[6] H. Zoog, et al., *Semicond. Sci. Technol*., **6**, C36 (1991)
[7] H. Peng, N. Kioussis, and G. J. Snyder, *Phys. Rev. B*., **89**, 195206 (2014)
[8] T. I. Lee, et al., *Adv. Mater*., **25**, 2920 (2013)
[9] W. Xu, et al., *Small* **4**, 888 (2008)
[10] Z. Zhu, et al., *Phy. Rev. Lett*. **119**, 106101 (2017)
[11] D. Liu, et al., *Nano Letters*, **18**, 4908 (2018)
[12] L. Xian, et al., *2D Mater*, **4**, 041003 (2017)
[13] B. Mayers and Y. Xia, J. *Mater. Chem*., **12**, 1875 (2002)
[14] J. Heyd, et al., J. Chem. Phys. **118**, 8207 (2003)
[15] G. Kresse and J. Furthumuller, *Phys. Rev. B,* **54**, 11169 (1996)
[16] J. P. Perdew, et al., *Phys. Rev. Lett*. **77**, 3865 (1996)
[17] S. Grimme, et al, *J. Chem. Phys.* **132**, 154104 (2010)
[18] H. J. Monkhorst, and J. D. Pack, *Phys. Rev. B,* **13**, 5188 (1976)
[19] S. Steiner et al., *Phys. Rev. B,* **93**, 224425 (2016)